Chemical Physics Letters 577 (2013) 27–31

Contents lists available at SciVerse ScienceDirect

Chemical Physics Letters

journal homepage: www.elsevier.com/locate/cplett

Vibrational energy transfer in $N(^2D) + N_2$ collisions: A quasiclassical trajectory study

B.R.L. Galvão [a], A.J.C. Varandas [b], J.P. Braga [a], J.C. Belchior [a,*]

[a] Departamento de Química-ICEx, Universidade Federal de Minas Gerais, Av. Antônio Carlos 6627, Pampulha, 31.270-901 Belo Horizonte, Minas Gerais, Brazil
[b] Departamento de Química, Universidade de Coimbra, 3004-535 Coimbra, Portugal

ARTICLE INFO

Article history:
Received 26 March 2013
In final form 20 May 2013
Available online 28 May 2013

ABSTRACT

Rate coefficients for the $N(^2D) + N_2$ collisions were calculated employing quasiclassical trajectories and the first available set of potential energy surfaces for such excited nitrogen interactions. The details of the vibrational energy transfer are discussed, such as the contributions from reactive and non-reactive trajectories as well as the contribution of each electronic symmetry. The calculated state-to-state and state-to-all rate coefficients show that deactivation is far more probable than excitation, and multi-quanta deactivation play an important role.

1. Introduction

Due to the large amount of nitrogen molecules available in Earth's atmosphere, several types of collisions involving this inert system may be important when free radicals, ions or other unstable species are present. As an example in the ionosphere, electronic impact is known to dissociate N_2 and generate excited nitrogen atoms [1]

$$N_2 + e^- \rightarrow N(^2D) + N + e^- \quad (1)$$

with some subsequent collisions of $N(^2D)$ being of fundamental importance, such as in the reaction with O_2 which is a major source of nitric oxide in the atmosphere [2].

The collisions of ground state nitrogen atoms with N_2 have received considerable theoretical attention (see Refs. [3–10], and references therein), due to its importance on the description of the extreme conditions achieved when objects enter the atmosphere at high speed [5], as well as for nitrogen containing plasmas. The excited nitrogen collisions should be also important but have been much less studied [11,12].

For a detailed modeling of such important species in the ionosphere, it would be therefore interesting to study the $N(^2D) + N_2$ collisions, which have not been carried out yet due to the lack of suitable potential energy surfaces (PES) to describe such an intricate interaction. In this work we calculate the contribution of both $^2A'$ and $^2A''$ electronic PESs for the dynamics and provide the first rate coefficients for the vibrational energy transfer process.

The paper is divided as follows: Section 2 presents the PESs utilized while in Section 3 the integration of quasiclassical trajectories is described. The results are discussed in Section 4, and the conclusions gathered in Section 5.

2. Potential energy surfaces

The interaction of $N(^2D)$ with N_2 gives rise to five different PESs [13]: 1,2 of $^2A'$ symmetry and 1,2,3 of $^2A''$. The $3^2A''$ can be safely discarded since it is highly repulsive and does not show low-lying intersections with lower PESs. The other four PESs were recently modeled in a global form [13,14] with the double many-body expansion (DMBE) method [15–17], using accurate *ab initio* energies of multi-reference configuration interaction quality with the Davidson correction (MRCI+Q) [18,19]. They are shown together in Figure 1, where the optimized linear path for the atom attack on the diatom is shown. Note that the two lowest sheets are degenerate at the global minimum, corresponding to the N_3 molecule in its $^2\Pi_g$ state. The transition state for the linear attack is also degenerate and is highlighted in the plot, lying 2.8 kcal mol^{-1} above the reactants [20].

The PESs are also displayed for a C_{2v} atom–diatom attack in Figure 2, where the minimum corresponding to the cyc-N_3 isomer and various conical intersections are also visible. In this plot the dissociation limit is presented at the left-hand side, since for acute angles the optimized bond lengths are very large. A barrier of 6.8 kcal mol^{-1} arises for the T-shaped attack, which is 4 kcal mol^{-1} higher than for the collinear one.

For each symmetry, a different methodology was used to model a double-sheeted PES ensuring a proper description of the conical intersections and dissociation limits. For the $^2A''$ symmetry, which

* Corresponding author. Fax: +55 31 3499 5700.
E-mail addresses: jadson@ufmg.br, jadsonbelchior@gmail.com (J.C. Belchior).

0009-2614
http://dx.doi.org/10.1016/j.cplett.2013.05.038

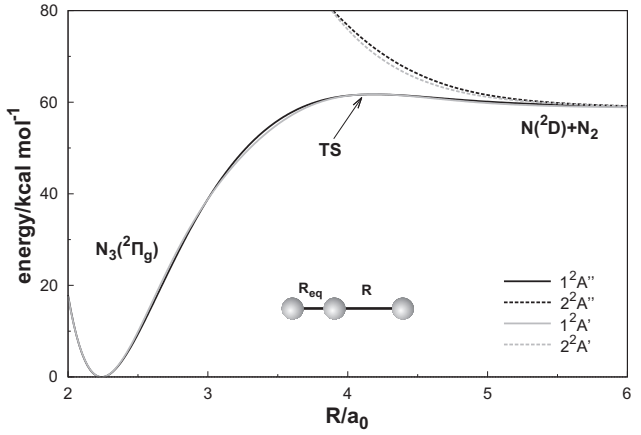

Figure 1. Potential energy profiles for the linear attack of a N(^2D) atom on a N_2 molecule with optimized diatomic bond length. The black lines correspond to the first two $^2A''$ states, while the gray ones to $^2A'$.

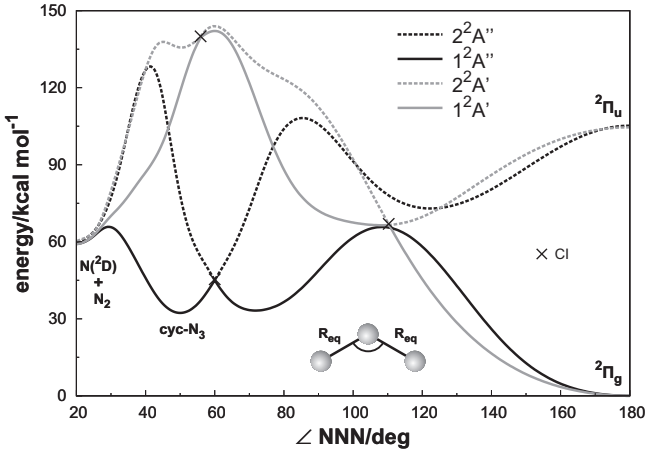

Figure 2. Potential energy profiles for optimized C_{2v} geometries. The crossing between surfaces of same symmetry are marked with a × symbol, while the notation for the lines is kept from Figure 1.

has a single crossing seam at D_{3h} configurations, the adiabatic surfaces could be simultaneously fitted using a method [21] that ensures their degeneracy along the intersection line. For the $^2A'$ symmetry, a 2 × 2 diabatic representation of the electronic Hamiltonian was proposed, which upon diagonalization gives the adiabatic PESs that accurately reproduce the calculated *ab initio* data [14].

3. Quasiclassical trajectories

The PESs here employed have already been tested in order to verify their validity for dynamical purposes. Such tests include studies of the nitrogen exchange reaction [14] both adiabatic by running trajectories on the lowest surfaces and non-adiabatic by using the trajectory surface hoping (TSH) method [22,23] for transitions to the excited state of same symmetry. It was concluded that nonadiabatic transitions could not make a significant impact on the rate coefficients, and therefore all trajectories here reported are independently integrated for each symmetry on the corresponding lowest adiabatic PES. In fact, we have tested the impact of running the trajectories starting on the upper sheets, and found no vibrational transition to take place, only small amounts of rotational energy is exchanged in this case. Also neglected are electronic transitions to the quartet state which are believed to be far less probable than the simple vibrational energy transfer here studied due to their spin-forbidden character. It should also be noted that the use of quasiclassical trajectories is justified by the large masses of the atoms involved [24].

For each adiabatic ground state ($1^2A'$ and $1^2A''$), trajectories were integrated for fixed temperatures and fixed value of the initial vibrational state (v_i) of the N_2 molecule using the QCT method [25,26]. The temperature was used for the sampling of the relative atom–diatom translational energy, as well as for sampling the rotational state of the reactant molecule (considering the appropriate ortho–para symmetry weights). The calculations used a time step of 0.2 fs with the reactants initially separated by 17 a_0, while the maximum value of the impact parameter (b_{max}) has been optimized by trial and error for each batch. After the trajectory has been completed, the final ro-vibrational state of the products were determined by the semiclassical quantization method [26].

The Monte-Carlo integrated rate coefficient for each process of vibrational energy transfer is given as the sum of the contribution of the two PESs ($k(T) = k_{^2A'}(T) + k_{^2A''}(T)$), with each term given by:

$$k_x^{i\to f}(T) = g_e(T)\left(\frac{8k_BT}{\pi\mu}\right)^{1/2}\pi b_{max}^2\frac{N^{i\to f}}{N} \tag{2}$$

where k_B is the Boltzmann constant, μ is the reduced mass of the reactants, and $N^{i\to f}/N$ is the fraction of $v_i \to v_f$ trajectories from the total number that has been integrated. The term $g_e(T)$ is the electronic degeneracy factor which has the high temperature limit of 1/5 but has here been calculated using its analytic form $g_e(T) = q_{N_3}/q_{N(^2D)}q_{N_2} : q_{N_3} = 2, q_{N_2} = 1,$ and $q_{N(^2D)} = 6 + 4\exp(-12.53\,K/T)$ are partition functions. The 68% error bars associated with the trajectories (shown in the graphs and tables) are given by $\Delta k_x^{i\to f} = k_x^{i\to f}\left(\frac{N-N^{i\to f}}{NN^{i\to f}}\right)^{1/2}$.

4. Results and discussion

Batches of 5×10^4 trajectories were integrated for the temperatures of $T = 750, 1000$ and 1250K and for even initial vibrational states of the N_2 molecule from 0 to 12 (and also for 20 and 30 in order to extend its range). The general properties of the state-to-state collisions are illustrated by showing the rate coefficients for the vibrational energy transfer $N(^2D) + N_2(v_i = 6) \to N(^2D) + N_2(v_f)$ in Figure 3 at $T = 1000$K, with separated contributions of each PES and from reactive (nitrogen atoms exchanged) and non-reactive events. As can be seen from this plot, the non-reactive events are more probable, a result that gets enhanced for lower temperatures and lower vibrational states, as can be expected since there is a reduced chance of overcoming the potential barrier for reaction (see Figure 1). It is also clear that the one-quantum transitions dominate the excitation process, and that its rate coefficient is much smaller than the deactivation one, where multi-quanta transitions are seen to be also important. Since we are interested on the energy transfer only, we have neglected the vibrationally-elastic rate coefficients, but it is worth mentioning that they are generally two orders of magnitude larger than the one-quantum ones. A curious feature is that reactive deactivation shows different patterns for each PES for $v_i = 6$: the $^2A'$ state shows a larger rate coefficient for a one-quantum transition than for multi-quanta ones, whereas in the $^2A''$ the highest probability arises for the $6 \to 0$ transition, thus showing the opposite v_f dependence.

In order to understand the above difference, we have calculated the average time that the trajectories spend inside the potential well (with potential energy lower by 1 kcal mol^{-1} or more than reactants) since, if the potential well is able to trap the system for a long time, there are more chances that the energy will be randomized among the degrees of freedom, with the final outcome

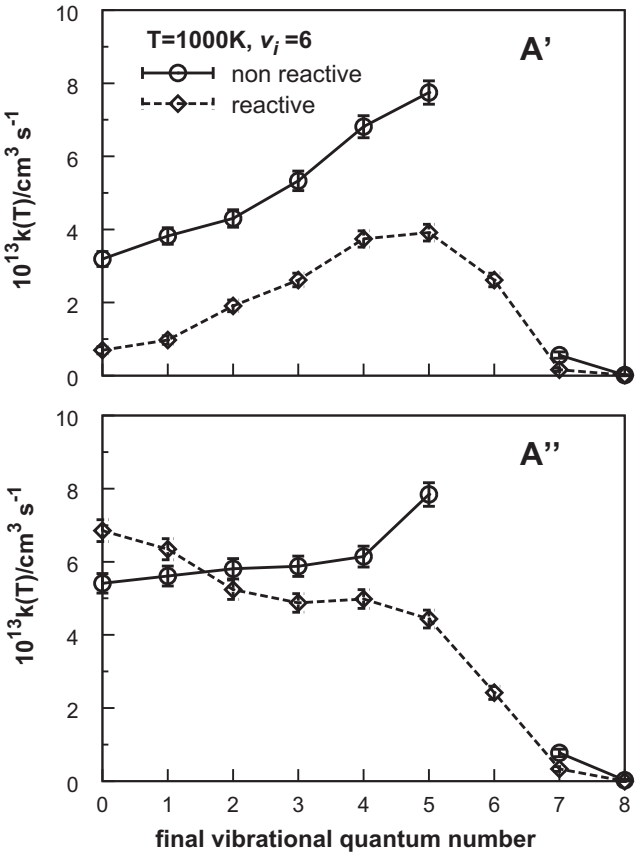

Figure 3. Rate coefficient for the $6 \rightarrow v_f$ vibrational energy transfer process for $T = 1000$K.

showing a reduced dependence on the initial state (i.e. the molecule "forgets" the initial state and populates others). This would be expected mostly in the reactive trajectories, as is the case, given that they must enter the potential well (while the non-reactive may not). Given that the $^2A''$ state holds the cyc $-$ N_3 well, while the $^2A'$ is mostly repulsive for C_{2v} configurations (see Figure 2), we can expect that $^2A''$ will hold the system longer and the above feature will therefore find a justification.

The average lifetime of such a complex was calculated as $\langle\tau\rangle = \sum_i^N \tau_i/N$, where τ_i is the time spent in the potential well for trajectory i, which is zero if the trajectory did not enter the well. For the batch at $T = 1000$K and $v_i = 6$, we have obtained $\langle\tau\rangle = 3.1$ fs for the $^2A'$ state, compared to 4.6fs on the $^2A''$ state (33% larger), thus corroborating our previous analysis.

The final results achieved by summing the $^2A'$ and $^2A''$ states and treating reactive and non-reactive events on an equal basis. This is shown in Figure 4 for all initial vibrational states calculated. Note that the trend regarding the excitation is maintained (only one-quantum and small), while for the deactivation process the different behaviors for each symmetry average out, keeping the general result that multi-quanta transitions are very important.

The state-to-all vibrational deactivation process ($v_i \rightarrow \sum v_f < v_i$) is shown in Figure 5 for the particular case of $T = 1000$K: here too the contributions from reactive and non-reactive processes on each PES are shown separately. For the non-reactive process, the contribution from the $^2A'$ and $^2A''$ PESs are similar over all initial vibrational states, whereas for the reactive case the $^2A''$ gives a larger contribution for $v_i > 6$. This may be attributed to the fact that the $^2A''$ PES has the possibility of another reaction path through a T-shaped attack (see Figure 2) while the $^2A'$ is largely repulsive for such geometries. Furthermore, a trajectory in the

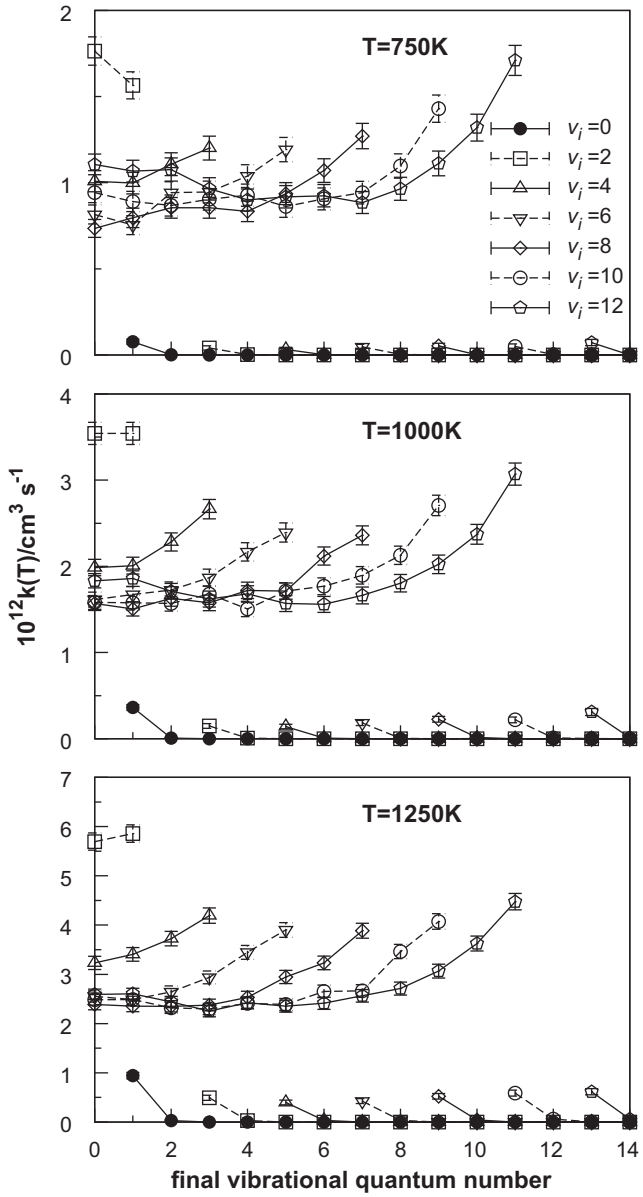

Figure 4. Rate coefficient for state-to-state vibrational energy transfer at $T = 1000$K.

$^2A''$ PES that forms a linear isomer, may transite to the cyclic well and from there yield exchanged products, thence contributing to the reactive part of the rate coefficient. Since the $^2A'$ PES does not present the cyclic isomer of N_3 none of the above exchange pathways will apply. All information gathered on state-to-all deactivation and excitation is given in Table 1, where the dominant role of the deactivation is seen to hold for all temperatures.

It is worth comparing the properties of the title reaction against the ones relative to the vibrational energy transfer of the ground state atom ($N(^4S) + N_2$) [27,24]. Since the potential for such an interaction is more repulsive, with an energy barrier of 45.9 kcal mol^{-1} for the exchange reaction, the rate coefficients are expected to be much lower. For example, the rate coefficients for vibrational energy transfer over the temperature range calculated in this letter are negligible for the $N(^4S)$ case, and for a direct comparison with Ref. [24], we have integrated trajectories for $v_i = 4$ at $T = 3400$K. For the state-to-all non-reactive deactivation and excitation the $N(^4S) + N_2$ rate coefficients are 1.6 and 4.6 (in $\times 10^{-13}$ cm^3 mol^{-1}) [24] respectively, whereas for the excited atom

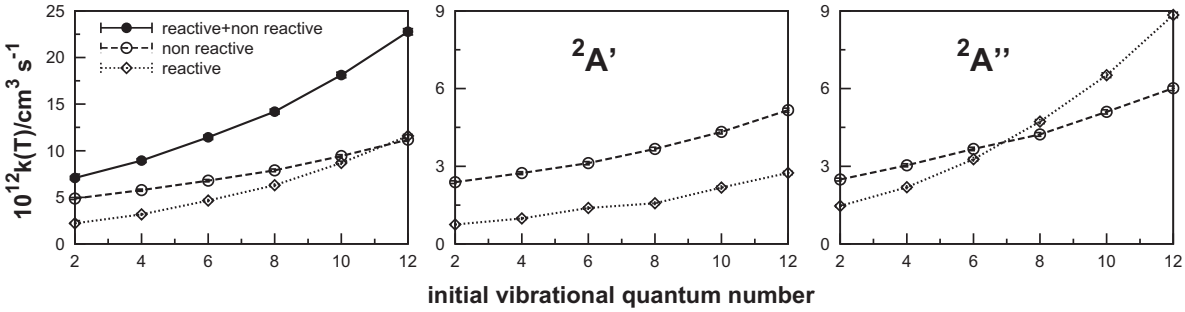

Figure 5. Rate coefficient for the vibrational deactivation process $N(^2D) + N_2(v_i) \rightarrow N(^2D) + N_2(\sum v_f < v_i)$ at $T = 1000$K. The first panel shows the total rate coefficient and the contribution from non-reactive and reactive trajectories, while the following panels give the contribution from each PES separately.

Table 1
Rate coefficients for the state-to-all vibrational energy transfer (in 10^{13} cm^3 mol^{-1}).

v_i	Deactivation $v_i \rightarrow \sum v_f < v_i$	Excitation $v_i \rightarrow \sum v_f > v_i$
T = 750 K		
0	–	0.8 ± 0.1
2	33 ± 1	0.4 ± 0.1
4	43 ± 1	0.3 ± 0.1
6	57 ± 2	0.5 ± 0.1
8	74 ± 2	0.5 ± 0.1
10	98 ± 2	0.5 ± 0.1
12	130 ± 2	0.7 ± 0.2
20	391 ± 5	3.2 ± 0.4
30	1257 ± 16	13.0 ± 1.8
T = 1000 K		
0	–	3.7 ± 0.3
2	71 ± 2	1.6 ± 0.3
4	89 ± 2	1.5 ± 0.3
6	114 ± 2	1.9 ± 0.3
8	142 ± 3	2.4 ± 0.3
10	181 ± 3	2.3 ± 0.3
12	228 ± 3	3.3 ± 0.4
20	560 ± 6	6.6 ± 0.7
30	1423 ± 25	24.0 ± 3.8
T = 1250 K		
0	–	9.7 ± 0.7
2	116 ± 2	5.3 ± 0.5
4	146 ± 3	4.4 ± 0.5
6	180 ± 3	4.6 ± 0.5
8	221 ± 4	5.7 ± 0.6
10	272 ± 4	6.6 ± 0.6
12	335 ± 4	6.8 ± 0.7
20	709 ± 7	14.5 ± 1.2
30	1595 ± 18	33.7 ± 3.0

we found 339 and 69, showing that they differ by one or two orders of magnitude. The $N(^2D)$ rate coefficients at $T = 750$K compare in magnitude with the $N(^4S)$ ones at much higher temperatures, namely around $T = 3400$K. Obviously, the importance of the collisions of the excited atom will depend on its concentration relatively to the ground state one, but given that $N(^2D)$ is known to be available in important atmospheric and plasma conditions, it would be worth paying attention to the excited atom, given the much higher rate coefficients and reactivity of such a state. Another interesting feature is that, for the ground state, the excitation process dominates over deactivation as opposed to the insignificant role played by the excitation for the excited atom. The latter result is also a particular contribution of the present theoretical analysis. Still in opposition to the excited state, the non-reactive collisions of $N(^4S)$ favor one-quantum vibrational transitions as can be found by comparing our results with the ones from Ref. [24].

Finally, the temperature dependence of the vibrational deactivation is shown in Figure 6, where a logarithmic curve is given

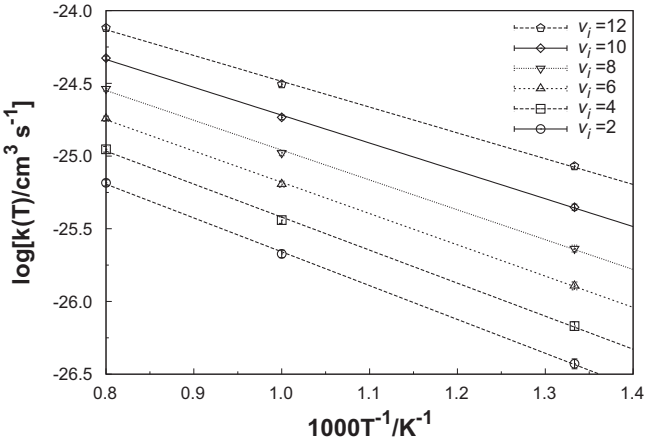

Figure 6. Arrhenius plot for the deactivation rate coefficients of the $v_i \rightarrow \sum v_f < v_i$ processes.

Table 2
Parameters obtained in a fit to an Arrhenius curve $k(T) = A\exp(-E_a/k_bT)$ for the state-to-all deactivation shown in Figure 6.

v_i	A [10^{10} cm^3 s^{-1}]	E_a[kcal mol^{-1}]
2	0.7359	4.6222
4	0.8832	4.5108
6	0.9954	4.2726
8	1.1257	4.0772
10	1.2486	3.8057
12	1.3687	3.5253

for the deactivation process from each calculated vibrational state. For convenience, the points were fitted to an Arrhenius law as shown by the lines in this graph. Despite the observed linear behavior as a function of temperature, it must be stressed that non-reactive events may not necessarily follow such a law (there is no clear energy barrier). In fact, we have even verified that it does not predict well the results for temperatures far from the range here considered (3400 K). Nevertheless, the resulting parameters are given in Table 2 and may be useful both for calculating the rate coefficients at intermediate temperatures in this range and curves for odd initial vibrational states, since their values show a fairly uniform progression.

5. Conclusions

We have performed the first theoretical predictions of the vibrational energy transfer in collisions between excited atomic

nitrogen and molecular nitrogen. Quasiclassical trajectories were employed using accurate potential energy surfaces, and the results for the rate coefficients discussed. It is found that deactivation dominates the energy transfer process and that multi-quanta transitions are important. Vibrational excitation behaves distinctly, with only one-quantum transfers appearing to matter.

Acknowledgments

B.R.L.G. thanks the Conselho Nacional de Desenvolvimento Científico e Tecnológico (CNPq) for the grant 150071/2013-2. The authors also acknowledge the financial support from CNPq and Fundação de Amparo Pesquisa do estado de Minas Gerais (FAPEMIG). The support from Fundação para a Ciência e Tecnologia, Portugal, to one of us (A.J.C.V.) is also gratefully acknowledged.

References

[1] R.W. Schunk, A.F. Nagy, Ionospheres: Physics, Plasma Physics, and Chemistry, Cambridge University Press, Cambridge, 2009.
[2] J.W. Duff, R.D. Sharma, J. Chem. Soc. Faraday Trans. 93 (1997) 2645.
[3] A. Laganà, E. Garcia, L. Ciccarelli, J. Phys. Chem. 91 (1987) 312.
[4] F. Esposito, M. Capitelli, C. Gorse, Chem. Phys. 257 (2000) 193.
[5] D. Wang, J.R. Stallcop, W.M. Huo, C.E. Dateo, D.W. Schwenke, H. Partridge, J. Chem. Phys. 118 (2003) 2186.
[6] D. Wang, W.M. Huo, C.E. Dateo, D.W. Schwenke, J.R. Stallcop, J. Chem. Phys. 120 (2004) 6041.
[7] F. Esposito, M. Capitelli, Chem. Phys. Lett. 418 (2006) 581.
[8] N.F. Lago, A. Laganà, R. Gargano, P. Barreto, J. Chem. Phys. 125 (2006) 114311.
[9] S. Rampino, D. Skouteris, A. Laganà, E. Garcia, A. Saracibar, Phys. Chem. Chem. Phys. 11 (2009) 1752.
[10] M. Panesi, R.L. Jaffe, D.W. Schwenke, T.E. Magin, J. Chem. Phys. 138 (2013) 044312.
[11] A. Laricchiuta, F. Pirani, G. Colonna, D. Bruno, C. Gorse, R. Celiberto, M. Capitelli, J. Phys. Chem. A 113 (2009) 15250.
[12] M. Capitelli, D. Bruno, G. Colonna, C. Catalfamo, A. Laricchiuta, J. Phys. D: Appl. Phys. 42 (2009) 194005.
[13] B.R.L. Galvão, A.J.C. Varandas, J. Phys. Chem. A 115 (2011) 12390.
[14] B.R.L. Galvo, P.J.S.B. Caridade, A.J.C. Varandas, J. Chem. Phys. 137 (2012) 22A515.
[15] A.J.C. Varandas, J. Mol. Struct. Theochem. 21 (1985) 401.
[16] A.J.C. Varandas, Adv. Chem. Phys. 74 (1988) 255.
[17] A.J.C. Varandas, in: A. Laganà, A. Riganelli (Eds.), Lecture Notes in Chemistry, vol. 75, Springer, Berlin, 2000, p. 33.
[18] H.-J. Werner, P.J. Knowles, J. Chem. Phys. 89 (1988) 5803.
[19] H.-J. Werner, P.J. Knowles, Chem. Phys. Lett. 145 (1988) 514.
[20] P. Zhang, K. Morokuma, A.M. Wodtke, J. Chem. Phys. 122 (2005) 014106.
[21] A.J.C. Varandas, A. Alijah, M. Cernei, Chem. Phys. 308 (2005) 285.
[22] J.C. Tully, R.K. Preston, J. Chem. Phys. 55 (1971) 562.
[23] A.I. Voronin, J.M.C. Marques, A.J.C. Varandas, J. Phys. Chem. A 102 (1998) 6057.
[24] P.J.S.B. Caridade, B.R.L. Galvão, A.J.C. Varandas, J. Phys. Chem. A 114 (2010) 6063.
[25] W.L. Hase et al., QCPE Bull. 16 (1996) 43.
[26] G.H. Peslherbe, H. Wang, W.L. Hase, Adv. Chem. Phys. 105 (1999) 171.
[27] B.R.L. Galvão, A.J.C. Varandas, J. Phys. Chem. A 113 (2009) 14424.